Systematic and causal corrections to the coherent potential approximation

M. Jarrell[1] and H. R. Krishnamurthy[2]
[1]*Department of Physics, University of Cincinnati, Cincinnati, Ohio 45221*
[2]*Department of Physics, IISc, Bangalore 560 012, India*
(Received 27 June 2000; published 7 March 2001)

The dynamical cluster approximation (DCA) is modified to include disorder. The DCA incorporates nonlocal corrections to local approximations such as the coherent potential approximation (CPA) by mapping the lattice problem with disorder, and in the thermodynamic limit, to a self-consistently embedded finite-sized cluster problem. It satisfies all of the characteristics of a successful cluster approximation. It is causal, preserves the point-group and translational symmetry of the original lattice, recovers the CPA when the cluster size equals one, and becomes exact as $N_c \to \infty$. We use the DCA to study the Anderson model with binary diagonal disorder. It restores sharp features and band tailing in the density-of-states, which reflect correlations in the local environment of each site. While the DCA does not describe the localization transition, it does describe precursor effects of localization.

DOI: 10.1103/PhysRevB.63.125102 PACS number(s): 71.23.An, 71.15.Mb

I. INTRODUCTION

The coherent potential approximation (CPA)[1–3] is a widely used method for treating disordered systems. Within the CPA, the problem is first averaged over all possible disorder configurations in an attempt to regain the translational invariance lost due to disorder. Then nonlocal correlations of the disorder potential are neglected leading to a self-consistent single-site approximation (like the Weiss mean-field theory of magnetism). It has been applied with great success to a variety of problems,[1–3] including *ab initio* calculations in disordered metallic alloys.[4]

Nevertheless, the CPA fails to provide a completely satisfactory theory for disordered systems.[3] As a single-site mean-field theory, it cannot account for the disorder induced, short-ranged but nonlocal, correlations due to the local order in the environment of each site responsible for band tailing and sharp structures in the density-of-states. There have been many attempts[5,6,3] to formulate nonlocal corrections to the CPA in which the lattice is mapped onto a self-consistently embedded finite-sized cluster. However, as argued clearly and in detail by Gonis,[3] these theories all fail in some significant way. A successful theory must be able to account for fluctuations in the local environment in a self-consistent way, become exact in the limit of large cluster sizes, and recover the CPA when the cluster size equals one. It must be easily implementable numerically and preserve the translational and point-group symmetries of the lattice. Finally, and most significantly, it should be fully causal so that the single-particle Green function and self-energy are analytic in the upper half-plane. No presently existing cluster extension of the CPA satisfies *all these requirements*.[3,7]

Recently, a new method called the dynamical cluster approximation (DCA)[8–10] was developed for ordered correlated systems such as the Hubbard model to add nonlocal corrections to the dynamical mean-field approximation. In this paper, we modify the DCA to include disorder and show that the resulting formalism satisfies all of the above stated requirements for a successful cluster extension of the CPA.

In the next section, we review the basic diagrammatic perturbation theory formalism for disordered systems. In Sec. III A we show that the CPA is equivalent to neglecting momentum conservation at all internal vertices of the diagrams, and in Sec. III B we introduce the DCA for disordered systems that systematically restores the momentum conservation relinquished by the CPA. In Sec. IV we show that the DCA satisfies each of the desired characteristics described above. In Sec. V we show results for the two-dimensional Anderson model with binary diagonal disorder. Finally in the Appendix we present an alternate way of viewing and justifying the disordered DCA algorithm developed in this paper, using the replica (or other) methods of disorder averaging.

II. BASIC FORMALISM

We consider an Anderson model with diagonal disorder, described by the Hamiltonian

$$H = \sum_{\langle ij \rangle, \sigma} t(C^{\dagger}_{i,\sigma} C_{j,\sigma} + C^{\dagger}_{j,\sigma} C_{i,\sigma}) + \sum_{i\sigma} (V_i - \mu) n_{i,\sigma}, \quad (1)$$

where $C^{\dagger}_{i,\sigma}$ creates a quasiparticle on site i with spin σ, $n_{i,\sigma} = C^{\dagger}_{i,\sigma} C_{i,\sigma}$. The disorder occurs in the local orbital energies V_i, which we assume are independent quenched random variables distributed according to some specified probability distribution $P(V)$. *The DCA formalism that we develop in this paper is a general method valid for any* $P(V)$. However, for illustrative purposes, for the specific calculations presented in this paper, we take $V_i = \pm V$ with equal probability 1/2 (binary disorder).

The effect of the disorder potential $\Sigma_{i\sigma} V_i n_{i,\sigma}$ can be described using standard diagrammatic perturbation theory (although we will eventually sum to *all* orders). It may be rewritten in reciprocal space as

$$H_{\rm dis} = \frac{1}{N} \sum_{i,\mathbf{k},\mathbf{k}',\sigma} V_i C^{\dagger}_{\mathbf{k},\sigma} C_{\mathbf{k}',\sigma} e^{i\mathbf{r}_i(\mathbf{k}-\mathbf{k}')}. \quad (2)$$

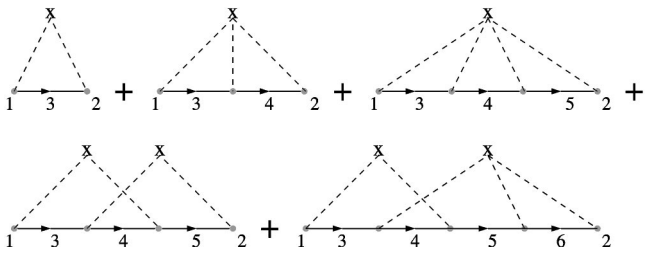

FIG. 1. The first few graphs in the irreducible self-energy of a diagonally disordered system. Each ○ represents the scattering of a state **k** from sites (marked *X*) with a local disorder potential distributed according to some specified probability distribution $P(V)$. The numbers label the **k** states.

The corresponding irreducible (skeletal) contributions to the self-energy may be represented diagrammatically[3] and are displayed in Fig. 1.

Here each ○ represents the scattering of an electronic Bloch state from a local disorder potential at some site represented by *X*. The dashed lines connect scattering events that involve the same local potential. In each graph, the sums over the sites are restricted so that the different *X* 's represent scattering from *different* sites. No graphs representing a single scattering event are included since these may simply be absorbed as a renormalization of the chemical potential μ.

Translational invariance and momentum conservation are restored by averaging over all possible values of the disorder potentials V_i. For example, consider the second diagram in Fig. 1, given by

$$\frac{1}{N^3}\sum_{i,\mathbf{k}_3,\mathbf{k}_4}\langle V_i^3\rangle G(\mathbf{k}_3)G(\mathbf{k}_4)e^{i\mathbf{r}_i\cdot(\mathbf{k}_1-\mathbf{k}_3+\mathbf{k}_3-\mathbf{k}_4+\mathbf{k}_4-\mathbf{k}_2)}, \tag{3}$$

where $G(\mathbf{k})$ is the disorder-averaged single-particle Green function for state **k**. The average over the distribution of scattering potentials $\langle V_i^3\rangle=\langle V^3\rangle$ independent of *i*. After summation over the remaining labels, this becomes

$$\langle V^3\rangle G(\mathbf{r}=0)^2\delta_{\mathbf{k}_1,\mathbf{k}_2}, \tag{4}$$

where $G(\mathbf{r}=0)$ is the local Green's function. Thus the second diagram's contribution to the self-energy involves only local correlations. Since the internal momentum labels always cancel in the exponential, the same is true for all noncrossing diagrams shown in the top half of Fig. 1.

Only the diagrams with crossing dashed lines are nonlocal. Consider the fourth-order diagrams such as those shown on the bottom left and upper right of Fig. 1. When we impurity average, we generate potential terms $\langle V^4\rangle$ when the scattering occurs from the same local potential (i.e., the third diagram) or $\langle V^2\rangle^2$ when the scattering occurs from different sites, as in the fourth diagram. When the latter diagram is evaluated, to avoid overcounting, we need to subtract a term proportional to $\langle V^2\rangle^2$ but corresponding to scattering from the same site. This term is needed to account for the fact that the fourth diagram should really only be evaluated for sites $i\neq j$! For example, the fourth diagram yields

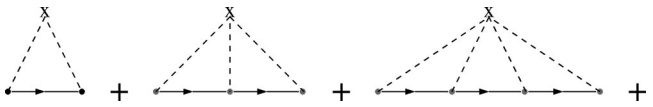

FIG. 2. The first few graphs of the CPA self-energy. Here the Green function line represents the average local propagator.

$$\left\langle \frac{1}{N^4}\sum_{i\neq j\mathbf{k}_3\mathbf{k}_4\mathbf{k}_5} V_i^2V_j^2 e^{i\mathbf{r}_i\cdot(\mathbf{k}_1+\mathbf{k}_4-\mathbf{k}_5-\mathbf{k}_3)}e^{i\mathbf{r}_j\cdot(\mathbf{k}_5+\mathbf{k}_3-\mathbf{k}_4-\mathbf{k}_2)} \times G(\mathbf{k}_5)G(\mathbf{k}_4)G(\mathbf{k}_3)\right\rangle. \tag{5}$$

Evaluating the disorder average $\langle\rangle$, we get the following two terms:

$$\frac{1}{N^4}\sum_{ij\mathbf{k}_3\mathbf{k}_4\mathbf{k}_5}\langle V^2\rangle^2 e^{i\mathbf{r}_i\cdot(\mathbf{k}_1+\mathbf{k}_4-\mathbf{k}_5-\mathbf{k}_3)}e^{i\mathbf{r}_j\cdot(\mathbf{k}_5+\mathbf{k}_3-\mathbf{k}_4-\mathbf{k}_2)} \times G(\mathbf{k}_5)G(\mathbf{k}_4)G(\mathbf{k}_3) - \frac{1}{N^4}\sum_{i\mathbf{k}_3\mathbf{k}_4\mathbf{k}_5}\langle V^2\rangle^2 e^{i\mathbf{r}_i\cdot(\mathbf{k}_1-\mathbf{k}_2)}G(\mathbf{k}_5)G(\mathbf{k}_4)G(\mathbf{k}_3). \tag{6}$$

Momentum conservation is restored by the sum over *i* and *j*; i.e., over all possible locations of the two scatterers. It is reflected by the Laue functions, $\Delta=N\delta_{\mathbf{k}+\ldots}$, within the sums

$$\frac{\delta_{\mathbf{k}_2,\mathbf{k}_1}}{N^3}\sum_{\mathbf{k}_3\mathbf{k}_4\mathbf{k}_5}\langle V^2\rangle^2 N\delta_{\mathbf{k}_2+\mathbf{k}_4,\mathbf{k}_5+\mathbf{k}_3} \times G(\mathbf{k}_5)G(\mathbf{k}_4)G(\mathbf{k}_3) - \frac{\delta_{\mathbf{k}_2,\mathbf{k}_1}}{N^3}\sum_{\mathbf{k}_3\mathbf{k}_4\mathbf{k}_5}\langle V^2\rangle^2 G(\mathbf{k}_5)G(\mathbf{k}_4)G(\mathbf{k}_3). \tag{7}$$

Since the first term in Eq. (7) involves convolutions of $G(\mathbf{k})$ it reflects nonlocal correlations. [Local contributions such as the second term in Eq. (7) can, if one so chooses, be combined together with the contributions from the corresponding local diagrams such as the third diagram in Fig. 1 by replacing $\langle V^4\rangle$ in the latter by the cumulant $\langle V^4\rangle-\langle V^2\rangle^2$.] Given the fact that different *X*'s must correspond to different sites, it is easy to see that all crossing diagrams must involve nonlocal correlations.

III. CLUSTER APPROXIMATIONS

A. The coherent potential approximation

In the CPA, nonlocal correlations involving different scatterers are ignored. Thus, in the calculation of the self-energy, we ignore all of the crossing diagrams shown on the bottom of Fig. 1; and retain only the class of diagrams such as those shown on the top representing scattering from a single local disorder potential. These diagrams are shown in Fig. 2.

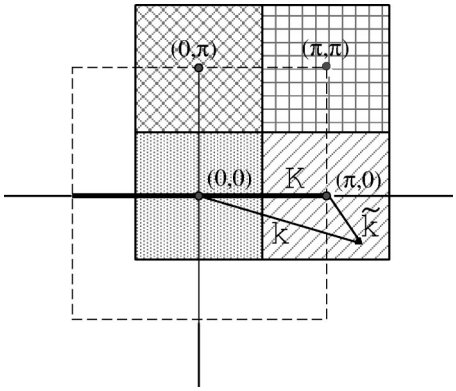

FIG. 3. $N_c=4$ cluster cells (shown by different fill patterns) that partition the first Brillouin zone (dashed line). Each cell is centered on a cluster momentum **K** (filled circles). To construct the DCA cluster, we map a generic momentum in the zone such as **k** to the nearest cluster point $\mathbf{K}=\mathbf{M}(\mathbf{k})$ so that $\tilde{\mathbf{k}}=\mathbf{k}-\mathbf{K}$ remains in the cell around **K**.

Employing diagrammatic arguments, it is easy to see that the CPA is fully equivalent to the neglect of momentum conservation at each internal vertex. This is accomplished by setting each Laue function within the sum [e.g., in Eq. (7)] to 1. We may then freely sum over the internal momenta, leaving only local propagators. All nonlocal self-energy contributions (crossing diagrams) must then vanish. For example, consider again the fourth graph. If we replace the Laue function $N\delta_{\mathbf{k}_1+\mathbf{k}_4,\mathbf{k}_5+\mathbf{k}_3}\rightarrow 1$ in Eq. (7), then the two contributions cancel and this diagram vanishes. Thus an alternate definition of the CPA,[11] in terms of the Laue functions Δ, is

$$\Delta=\Delta_{\mathrm{CPA}}=1. \tag{8}$$

That is, the CPA is equivalent to the neglect of momentum conservation at all internal vertices of the disorder-averaged irreducible graphs.

B. The dynamical cluster approximation

The DCA systematically restores the momentum conservation at internal vertices, which was relinquished by the CPA, and so incorporates nonlocal corrections. This is done by dividing the Brillouin zone into N_c equal cells, as shown in Fig. 3 and requiring that momentum be partially conserved for momentum transfers between the coarse graining cells shown in Fig. 3, but ignored for momentum transfers within each cell. This may be accomplished by employing the Laue functions

$$\Delta=\Delta_{\mathrm{DCA}}=N_c\delta_{\mathbf{M}(\mathbf{k}_1)+\mathbf{M}(\mathbf{k}_2),\mathbf{M}(\mathbf{k}_3)+\mathbf{M}(\mathbf{k}_4)\ldots}, \tag{9}$$

where $\mathbf{M}(\mathbf{k})$, illustrated in Fig. 3, maps the momenta **k** to the nearest cluster momenta **K**. Δ_{DCA} becomes one when $N_c=1$ since then all momenta are mapped to the zone center by **M**. Thus the CPA is recovered in this limit. Furthermore, as N_c becomes large, the exact result is recovered since $\lim_{N_c\rightarrow\infty}\mathbf{M}(\mathbf{k})=\mathbf{k}$ for all momenta **k**.

If we employ the DCA Laue function in each of the self-energy diagrams shown in Fig. 1 then we may freely sum over the momenta within each coarse-graining cell shown in Fig. 3. As illustrated in Fig. 4 for a fourth-order graph, this leads to the replacement of the lattice propagators $G(\mathbf{k}_1),G(\mathbf{k}_2),\ldots$ by coarse-grained propagators $\bar{G}(\mathbf{K}),\bar{G}(\mathbf{K}'),\ldots$ which are given by

$$\bar{G}(\mathbf{K})\equiv\frac{N_c}{N}\sum_{\tilde{\mathbf{k}}}G(\mathbf{K}+\tilde{\mathbf{k}}), \tag{10}$$

where N is the number of points of the lattice, N_c is the number of cells in the cluster, and the $\tilde{\mathbf{k}}$ summation runs over the momenta of the cell about the cluster momentum **K** (cf. Fig. 3).

As N_c increases from one, systematic nonlocal corrections to the CPA self-energy are introduced. To see this, recall that the self-energy is a functional of the Green function. According to Nyquist's sampling theorem,[12] to reproduce correlations of length $\lesssim L/2$ in the Green function and corresponding self-energy, we only need to sample the reciprocal space at intervals of $\Delta k\approx 2\pi/L$. Knowledge of these Green functions on a finer scale in momentum is then Δk unnecessary, and may be discarded to reduce the complexity of the problem. Thus the cluster self-energy will be constructed from the *coarse-grained average* of the single-particle Green's function within the cell centered on the cluster momenta. For short distances $r\lesssim L/2$, where L is now the linear size of the cluster, the Fourier transform of the Green's function $\bar{G}(r)\approx G(r)+\mathcal{O}[(r\Delta k)^2]$, so that short-ranged correlations are reflected in the irreducible quantities constructed from $\bar{G}$; whereas, longer ranged correlations $r>L/2$ are cut off by the finite size of the cluster.[9]

We show in the Appendix that free-energy arguments presented previously[9] apply to the disordered case as well. In particular, the DCA estimate of the lattice free energy is minimized by the choice $\Sigma(\mathbf{k},\omega)=\bar{\Sigma}[\mathbf{M}(\mathbf{k}),\omega]$.

Algorithm: With the substitution $\Delta\rightarrow\Delta_{\mathrm{DCA}}$, most of the diagrams represented in Fig. 1 remain. However, the complexity of the problem is greatly reduced since the nontrivial sums involve only the cluster momenta K (numbering N_c instead of N). Furthermore, since these diagrams are the same as those from a finite-sized periodic cluster of N_c sites, we can easily sum this series to all orders by numerically solving the corresponding cluster problem. The resulting algorithm is as follows (*for notational convenience the frequency arguments are not displayed below*):

(1) Make a guess for the impurity-averaged cluster self-energy $\bar{\Sigma}(\mathbf{K})$, usually zero.

(2) Calculate the coarse-grained cluster Green functions

$$\bar{G}(\mathbf{K})=\frac{N_c}{N}\sum_{\tilde{\mathbf{k}}}\frac{1}{\omega+\mu-\epsilon_{\mathbf{K}+\tilde{\mathbf{k}}}-\bar{\Sigma}(\mathbf{K})}. \tag{11}$$

(3) Calculate the cluster-excluded propagator $\mathcal{G}(\mathbf{K})=1/[1/\bar{G}(\mathbf{K})+\bar{\Sigma}(\mathbf{K})]$. The introduction of $\mathcal{G}(\mathbf{K})$ is necessary to avoid overcounting diagrams on the cluster.

(4) Fourier transform $\mathcal{G}$ to the real-space matrix representation of the cluster problem, [i.e., write $\mathcal{G}_{n,m}$

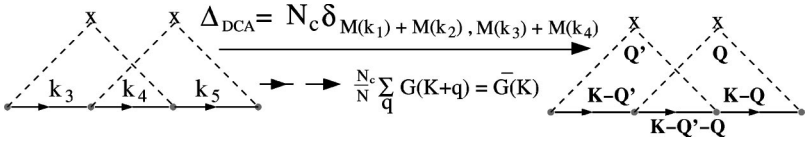

FIG. 4. Use of the DCA Laue function Δ_{DCA} leads to the replacement of the lattice propagators $G(\mathbf{k}_1), G(\mathbf{k}_2), \ldots$ by coarse grained propagators $\bar{G}(\mathbf{K}), \bar{G}(\mathbf{K}'), \ldots$.

$=\Sigma_{\mathbf{K}}\mathcal{G}(\mathbf{K})\exp i\mathbf{K}\cdot(\mathbf{r}_n-\mathbf{r}_m)]$ hence the disorder potential may be represented as a diagonal matrix $\mathbf{V}$ (with elements V_n on the cluster sites labeled by n) and form a new estimate of the disorder-averaged cluster Green function matrix

$$\mathbf{G}=\langle(\mathcal{G}^{-1}-\mathbf{V})^{-1}\rangle, \tag{12}$$

where the average $\langle\rangle$ indicates an average over disorder configurations on the cluster.[13]

(5) Transform back to the cluster reciprocal space and form a new estimate of the self-energy $\bar{\Sigma}(\mathbf{K})=1/\mathcal{G}(\mathbf{K})-1/G(\mathbf{K})$.

(6) Repeat, starting from (2), until $\bar{\Sigma}(\mathbf{K})$ converges to the desired accuracy.

The algorithm recovers the CPA for $N_c=1$ and becomes exact when $N_c\to\infty$.

IV. CHARACTERISTICS OF THE DCA

In Ref. 3 Gonis discusses the CPA, and various methods to incorporate nonlocal corrections. He lists the most important characteristics of a successful cluster theory. A successful theory must be able to account for fluctuations in the local environment in a self-consistent way, become exact in the limit of large cluster sizes, and recover the CPA when the cluster size becomes one. It must be straightforward to implement numerically and preserve the full point-group symmetry of the lattice. Finally, and most significantly, it should be fully causal so that the single-particle Green function and self-energy are analytic in the upper-half-plane. In the next two sections, we demonstrate that the DCA satisfies each of these requirements.

The limits $N_c\to1$ and $N_c\to\infty$: As mentioned above, the DCA recovers the CPA for $N_c=1$. When $N_c=1$, $\mathbf{K}=0$, and $\tilde{\mathbf{k}}=\mathbf{k}$. Then the DCA algorithm reduces to the self-consistent *scalar equations* (in contrast to the DCA, which involves matrix equations):

$$\bar{G}=\frac{1}{N}\sum_{\mathbf{k}}\frac{1}{\omega+\mu-\epsilon_{\mathbf{k}}-\bar{\Sigma}}, \tag{13}$$

$$\mathcal{G}^{-1}=1/\bar{G}+\bar{\Sigma}, \tag{14}$$

$$\bar{G}=\langle(\mathcal{G}^{-1}-V)^{-1}\rangle, \tag{15}$$

which together correspond exactly to the prescription for CPA,[3] and are easily solved, for example by iteration.

As $N_c\to\infty$ the DCA becomes exact, including correlations over all length scales. For, the DCA Laue function requires complete momentum conservation in this limit, i.e., $[\mathbf{K},\bar{G}(\mathbf{K})]\equiv[\mathbf{k},G(\mathbf{k})]$, hence $\mathcal{G}=1/(\omega+\mu-\epsilon_{\mathbf{k}})$, which is the bare lattice Green function so that Eq. (12) amounts to solving the problem by exact diagonalization.

Causality: It is easy to show that this algorithm is fully causal.[9]

For our purposes, this is equivalent to requiring that all the retarded propagators and self-energies are Herglotz, or analytic in the upper-half-plane. Since the diagrams which describe the DCA cluster problem are isomorphic to those of a real finite-size periodic cluster, the corresponding impurity averaged cluster self-energy shares the causal properties of this system. Furthermore, the coarse graining step (2) cannot violate causality, since the sum of analytic functions is analytic. The only ''suspect'' step is the cluster-exclusion step (3), thus we must show that the imaginary part of $\mathcal{G}$ is negative semidefinite. The essential steps of the argument are sketched in Fig. 5. The imaginary part of $\mathcal{G}(\mathbf{K},\omega)=[\bar{G}(\mathbf{K},\omega)^{-1}+\bar{\Sigma}(\mathbf{K},\omega)]^{-1}$ is negative provided that $\mathrm{Im}[\bar{G}(\mathbf{K},\omega)^{-1}]\geqslant-\mathrm{Im}\,\bar{\Sigma}(\mathbf{K},\omega)$. $\bar{G}(\mathbf{K},\omega)$ can be written as $\bar{G}(\mathbf{K},\omega)=(N_c/N)\Sigma_{\tilde{\mathbf{k}}}(z_{\mathbf{K}+\tilde{\mathbf{k}}})^{-1}(\omega)$, where the $z_{\mathbf{K}+\tilde{\mathbf{k}}}(\omega)$ are complex numbers with a positive semidefinite imaginary part $-\mathrm{Im}\,\bar{\Sigma}(\mathbf{K},\omega)$. For any $\mathbf{K}$ and ω, the set of points $z_{\mathbf{K}+\tilde{\mathbf{k}}}(\omega)$ are on a segment of the dashed *horizontal* line in the upper-half-plane due to the fact that the imaginary part is *independent* of $\tilde{\mathbf{k}}$. The mapping $z\to1/z$ maps this line segment onto a segment of the dashed circle shown in the lower-half-plane. $\bar{G}(\mathbf{K},\omega)$ is obtained by summing the points on the circle segment, yielding the empty dot that must lie *within* the dashed circle. The inverse necessary to take $\bar{G}(\mathbf{K},\omega)$ to $1/\bar{G}(\mathbf{K},\omega)$ maps this point onto the empty dot in the upper-half-plane, which must lie *above* the dashed line. Thus, the imaginary part of $\bar{G}(\mathbf{K},\omega)^{-1}$ is greater than or equal to $-\mathrm{Im}\,\bar{\Sigma}(\mathbf{K},\omega)$. This argument may easily be extended for $\mathcal{G}(z)$ for any z in the upper-half-plane. Thus $\mathcal{G}$ is completely analytic in the upper-half-plane.

Preservation of the lattice symmetry: Since the DCA is formulated in reciprocal space, it preserves the translational symmetry of the system. However, care must be taken when selecting the coarse-graining cells to preserve the point-group symmetries of the lattice. For example, the calcula-

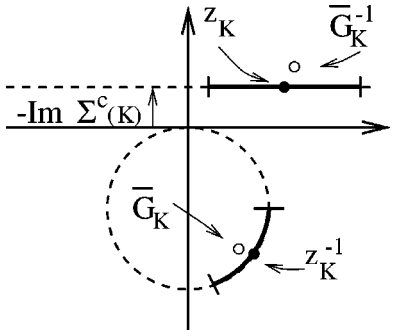

FIG. 5. Illustration of the essential steps of the proof that the DCA is causal (see the text).

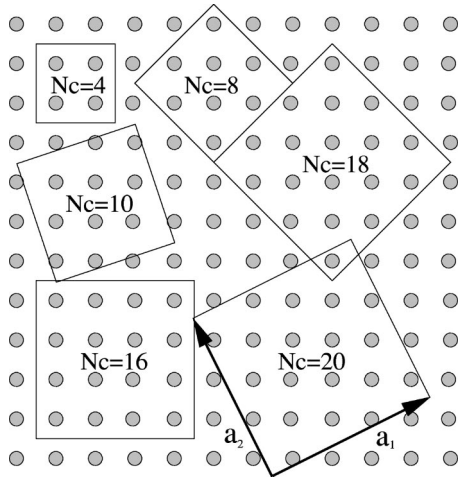

FIG. 6. Different tile sizes and orientations. The tiling principal translation vectors, $\mathbf{a}_1$ and $\mathbf{a}_2$, form two sides of each tiling square (illustrated for the $N_c=20$ tiling). For square tile geometries, $a_{2x}=-a_{1y}$ and $a_{2y}=a_{1x}$.

tions presented in Sec. V are done for a simple square lattice. Both it and its reciprocal lattice have a C_{4v} symmetry with eight point-group operations. We must choose a set of coarse-graining cells, which preserve this point-group symmetry. This may be done by tiling the real lattice with squares, and using the **K** points that correspond to the reciprocal space of the tiling centers. For large V, an important configuration of the half-filled system is all of the sites that have $V_i=-V$ occupied and $V_i=+V$ unoccupied. To retain this configuration on the cluster, when $N_c>1$ we will choose N_c even.

Square tilings with an even number of sites include $N_c=4,8,10,16,18,20,26,32,34,36,\ldots$. The first few are illustrated in Fig. 6. The relation between the principal lattice vectors of the lattice centers, $\mathbf{a}_1$ and $\mathbf{a}_2$, and the reciprocal lattice takes the usual form $\mathbf{g}_i=2\pi\mathbf{a}_i/|\mathbf{a}_1\times\mathbf{a}_2|$, with $\mathbf{K}_{nm}=n\mathbf{g}_1+m\mathbf{g}_2$ for integer n and m. For tilings with either $a_{1x}=a_{1y}$ (corresponding to $N_c=8,18,32,\ldots$) or one of a_{1x} or a_{1y} zero (corresponding to $N_c=1,4,16,36,\ldots$), the principal reciprocal lattice vectors of the coarse-grained system either point along the same directions as the principal reciprocal lattice vectors of the real system or are rotated from them by $\pi/4$. As a result equivalent momenta **k** are always mapped to equivalent coarse-grained momenta **K**. An example for $N_c=8$ is shown in Fig. 7. However, for $N_c=10,20,26,34,\ldots$, the principal reciprocal lattice vectors of the coarse-grained system do not point along a high-symmetry direction of the real lattice. Since all points within a coarse-graining cell are mapped to its center **K**, this means that these coarse graining choices violate the point-group symmetry of the real system. This is illustrated for $N_c=10$ in Fig. 7, where the two open dots, resting at equivalent points in the real lattice, fall in inequivalent coarse graining cells and so are mapped to inequivalent **K** points. Thus the tilings corresponding to $N_c=10,20,26,34,\ldots$ violate the point-group symmetry of the real lattice system and should be avoided.

An efficient numerical algorithm for disorder averaging:

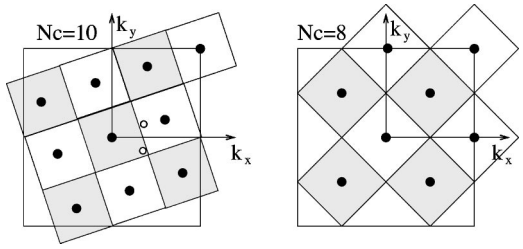

FIG. 7. The coarse-graining cells for $N_c=8$ and 10 each centered on a coarse-grained momenta **K** represented as black filled dots. For $N_c=8$ equivalent momenta **k** are always mapped to equivalent coarse-grained momenta **K**. However, this is not true for $N_c=10$ where, for example, the two equivalent momenta shown by open dots are mapped to inequivalent coarse-grained momenta.

The implementation of the DCA clearly requires an efficient algorithm for disorder averaging on a cluster of size N_c. (Needless to say, this particular aspect is common to all approaches where disorder averaging is involved.) Even for a system with binary diagonal disorder, where each site can acquire only one of two values for the potential ($\pm V$) the total number of disorder configurations is 2^{N_c}, which grows exponentially with N_c. For a generic quenched disorder, the probability of the various disorder configurations are determined by the specified $P(V)$; whereas, for annealed disorder, the probability of a configuration depends upon an effective Boltzmann factor determined by the electronic partition function for that particular disorder configuration.[9]

In this section, we propose an approach to carrying out the disorder averaging by statistically sampling disorder configurations using a Markov process. For systems with quenched disorder, one could also sample random configurations of the disorder potentials and calculate the corresponding Green's function using matrix inversion. A significant advantage of the Markov technique is that it may be easily modified to treat either quenched or annealed disorder.[9]

In a Markov process, each disorder configuration depends upon the previous configurations. To evolve from one configuration to another, we will propose local changes in the disorder potentials. These changes are accepted with some probability determined by either the effective Boltzmann factor,[9] for annealed disorder, or the probability distribution $P(V_i)$, for quenched disorder. If we accept such a change in one of the disorder potentials, say on site l, then the new Green's function matrix $G'_{n,m}$ depends on the previous Green's function matrix $G_{n,m}$ through the matrix relationship (*where, once again, for notational convenience, the frequency arguments are not displayed*)

$$\mathbf{G}'^{-1}-\mathbf{G}^{-1}=\mathbf{V}-\mathbf{V}'. \tag{16}$$

Since we change on the potential on the site l and the matrices $\mathbf{V}$ and $\mathbf{V}'$ are diagonal, their difference $\delta\mathbf{V}=\mathbf{V}-\mathbf{V}'$ is a diagonal matrix with only the lth diagonal element finite. Then

$$G'_{n,m}=G_{n,m}+G_{n,l}\delta V_l G'_{l,m}. \tag{17}$$

If we set $l=n$ in Eq. (17), we get

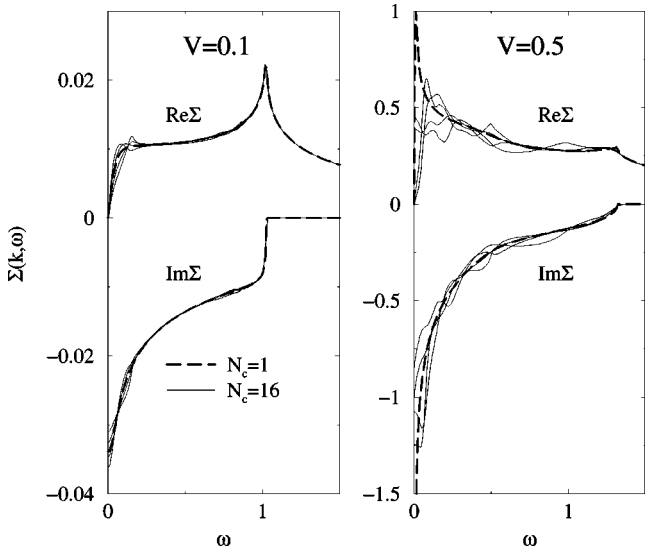

FIG. 8. The self-energy $N_c=1$ and for $N_c=16$ for different values of **K** for $V=0.1$ (left) and $V=0.5$ (right). The thin lines show $\overline{\Sigma}(\mathbf{K},\omega)$ for $\mathbf{K}=(0,0)$, $\mathbf{K}=(0,\pi)$, $\mathbf{K}=(\pi/2,\pi/2)$, and $\mathbf{K}=(\pi/2,0)$, plotted vs ω for $N_c=16$. For $V=0.1$ the self-energy at the different values of **K** is essentially the same as the $N_c=1$ result. For $V=0.5$, they differ significantly, indicating that the momentum dependence of the self-energy increases with V.

$$G'_{l,m}=\frac{G_{l,m}}{1-G_{l,l}\delta V_l}. \tag{18}$$

If we substitute this result back into Eq. (17), we get

$$G'_{n,m}=G_{n,m}+G_{n,l}\frac{\delta V_l}{1-G_{l,l}\delta V_l}G_{l,m} \tag{19}$$

an equation that requires roughly N_c^2 operations to evaluate[14] for each frequency.

Because the technique involves importance sampling, it is likely to miss rare configurations of disorder, and any special physics that arises from such configurations, such as Lifshitz tails in the density-of-states (DOS). However, when these configurations are well known, we can easily adapt this method to include them. This may be done by excluding them from the sampling, and then including the corresponding configurations in the sample with the appropriate reweighting.

V. RESULTS

A. Single-particle properties

To illustrate the algorithm discussed above, we present calculations on a two-dimensional square lattice system with $t=0.25$ and binary random disorder so that $V_i=\pm V$ with equal probability. No tricks are used to force the algorithm to remain causal such as renormalizing the spectrum or cutting off any negative tails of the density-of-states.

The self-energy is plotted in Fig. 8 for $N_c=1$ and for $N_c=16$ for different values of **K** for $V=0.1$ (left) and $V=0.5$ (right). For $V=0.1$ the self-energy for $N_c=16$ has very little momentum dependence, thus the different curves fall atop of one another. They also are hence very close to the self-energy for $N_c=1$ (the CPA result) indicating that it is a very good approximation for the self-energy when V is small. However, for larger $V=0.5$, the self-energy curves at different values of K for $N_c=16$ differ considerably from each other and from the CPA self-energy obtained with $N_c=1$. Thus, as V increases, nonlocal corrections clearly become important and are expressed in the momentum dependence of the self-energy.

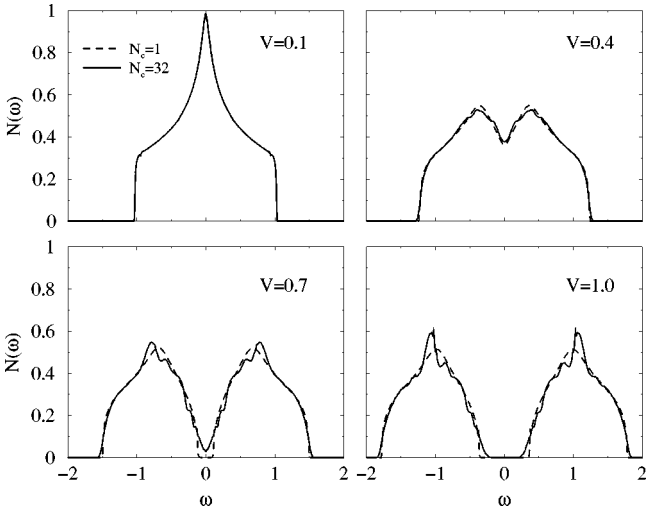

FIG. 9. The density-of-states for $N_c=1$ and for $N_c=32$ for four values of disorder potential V.

As shown in Fig. 9 (top left) the single-particle density-of-states is essentially independent of N_c for $V=0.1$; however, for $V=1.0$, the density-of-states depends strongly upon N_c. In particular the gap around $\omega=0$, which is sharp for $N_c=1$, is partially filled in. The top and bottom of the band also acquire tails as N_c increases. When $N_c>1$, the density-of-states acquires several additional structures, which correspond to important local configurations of the disorder. The additional features and the band tails are absent in the CPA and believed to be due to local order in the environment of each site.[3]

B. (Absence of) localization

Despite its advantages over the CPA as discussed above, one feature that the DCA shares with the CPA and similar self-consistent cluster methods is its limited ability to take into account localization effects.[15–17] To show this, we measure the probability that an electron remains at site l for all time:[15,16]

$$P(\infty)=\lim_{t\to\infty}\langle|G(l,l,t)|^2\rangle=\lim_{\eta\to 0}\frac{\eta}{\pi}\int_{-\infty}^{\infty}d\epsilon\langle|G_{l,l}(\epsilon+i\eta)|^2\rangle. \tag{20}$$

As shown in Refs. 15 and 16 $P(\infty)$ is expected to be nonzero as long as there are a thermodynamically significant fraction of localized states in the spectrum of eigenstates of the disordered system. In one and two dimensions this is expected to happen for arbitrarily small but thermodynami-

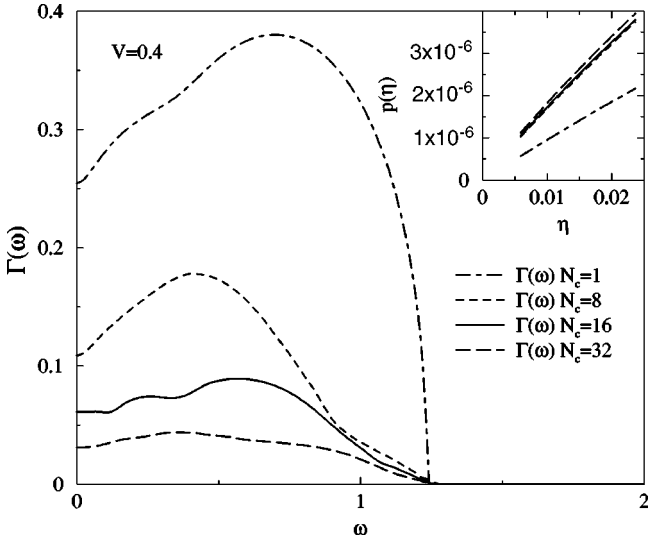

FIG. 10. The local hybridization rate when $V=0.4$ for several values of N_c. The probability that the electron remains localized $p(\eta\rightarrow 0)$, when $\epsilon=0$ (half-filling) is shown in the inset. As $\eta\rightarrow 0$, $p(\eta)$ extrapolates to zero indicating the lack of localization.

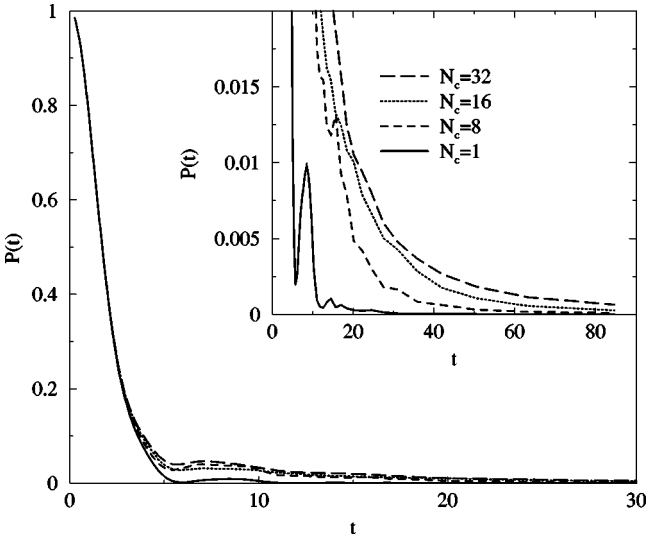

FIG. 11. The probability that an electron on a site l remains after a time t, $P(t)=\langle|G(l,l,t)|^2\rangle$ for several values of N_c when $V=0.4$.

cally significant disorder. Since the cluster is formed by coarse graining the real-lattice problem in reciprocal space, local quantities on the cluster and the real lattice correspond one-to-one. Thus, to test for localization, we need only apply formula (20) for each site on the cluster. Making this substitution and introducing the local coarse-grained (but not disorder averaged) spectral function, $\overline{A}(l,\omega)=-(1/\pi)\mathrm{Im}\,\overline{G}_{l,l}(\omega)$, Eq. (20) becomes

$$P(\infty)=\lim_{\eta\rightarrow 0}p(\eta)$$

$$=\lim_{\eta\rightarrow 0}\frac{-2i\eta}{N_c}\sum_l\int_{-\infty}^{\infty}d\omega\,d\omega'\left\langle\frac{\overline{A}(l,\omega)\overline{A}(l,\omega')}{\omega-\omega'-2i\eta}\right\rangle. \tag{21}$$

$p(\eta)$ is plotted versus η in the inset to Fig. 10 for the half-filled model when $V=0.4$. The $p(\eta)$ extrapolates to zero, indicating the lack of localization.

This result can be understood from either a diagrammatic perspective or by carefully assessing the cluster problem. As is well known,[17] the crossing diagrams, especially those that involve many crossings, describe the coherent backscattering of electrons which are responsible for localization. Hence the CPA, which includes only noncrossing diagrams, cannot describe localization. Within the DCA, however, for $N_c>1$ *some crossing graphs are restored*. Within each diagram, each X represents scattering from a distinct site. Since there are only N_c sites on the cluster, the maximally crossed DCA graphs can have at most N_c crossings. Since all states are expected to be localized in the two-dimensional disordered system, apparently an infinite number of crossings are needed to describe localization diagrammatically. From the perspective of the cluster, this result is not surprising since each site on the cluster is coupled to a noninteracting translationally invariant host into which electrons can escape. Thus, if the density-of-states is finite at some energy, then the corresponding states cannot be localized unless the hybridization rate at that energy between the cluster and the host vanishes.

As described in Ref. 10, the hybridization rate between the cluster and its host is given by

$$\Gamma(\mathbf{K},\omega)=\mathrm{Im}\left(\frac{1}{\overline{G}(\mathbf{K},\omega)}+\overline{\Sigma}(\mathbf{K},\omega)\right). \tag{22}$$

The net hybridization rate to a site on the cluster [the $\mathbf{K}$-integrated $\Gamma(\mathbf{K},\omega)$] is plotted in Fig. 10 when $V=0.4$ for several values of N_c. It remains finite over the entire region where the corresponding density-of-states, shown in Fig. 9, is finite. This is consistent with the lack of localization demonstrated in the inset.

We note that the hybridization falls as N_c increases [for large N_c, $\Gamma(\mathbf{K},\omega)\sim\mathcal{O}(1/N_c)$[10]] especially at the band edges, although, given that it is defined entirely in terms of disorder-averaged propagators, it is still unlikely to be sensitive to localization effects. However, the number of diagrammatic crossings in two-particle properties (such as the conductivity) which are strongly affected by localization effects, does increase with N_c even within the DCA. Thus, it is likely that disordered DCA can describe the precursor effects of localization. Some evidence for this can be seen in the (finite time) probability that an electron on a site l remains after a time t, $P(t)=\langle|G(l,l,t)|^2\rangle$. As shown in Fig. 11, for $N_c=1$, this probability falls quickly with time. The long-time behavior is shown in the inset. As N_c increases, the electron remains localized for longer times. Hence one can hope that a careful finite-size scaling study of two-particle properties within the disordered DCA can even capture some aspects of the localization transition.

VI. CONCLUSION

We have developed a modification of the dynamical cluster approximation to treat disordered systems. This formalism satisfies all of the characteristics of a successful cluster approximation. It is causal, preserves the point-group and translational symmetry of the original lattice, recovers the CPA when the cluster size goes to one, and becomes exact as $N_c \rightarrow \infty$. Like the CPA the problem is disorder averaged and has a simple diagrammatic formulation. It is easy to implement numerically and restores sharp features and band tailing in the DOS which reflect correlations in the local environment of each site. Although the DCA does not capture the localization transition, it does describe the precursor effects of localization. It systematically restores the crossing graphs known to be responsible for localization, and might be able to access the localization transition itself via an appropriate finite-size scaling analysis of two-particle properties that remains to be developed.

The DCA formalism we have discussed here can also be extended to problems with *disorder and interactions* simply by incorporating interaction diagrams in the self-energy. This is also discussed in the Appendix. The DCA should be able to provide a good description of localization effects at finite temperatures in such contexts. For, in such cases the scattering processes are partially inelastic, so that the coherent back scattering disappears after a characteristic inelastic-scattering time.[18] In this time only a finite number of back-scattering processes can occur so only a finite number of diagrammatic crossings are needed to describe the finite-temperature physics, and these are captured in the DCA.

ACKNOWLEDGMENTS

This work was initiated in conversations with B. L. Gyorffy. It is a pleasure to acknowledge useful discussions with F. P. Esposito, A. Gonis, M. Hettler, D. E. Logan, and M. Ma. This work was supported in part by NSF Grant Nos. DMR-9704021, DMR-9357199, and PHY94-07194 and by PRF Grant No. ACF-PRF 33611-AC6. This research was supported in part by NSF cooperative agreement No. ACI-961020 through computing resources provided by the National Partnership for Advanced Computational Infrastructure at the San Diego Supercomputer Center.

APPENDIX: DISORDER-DCA FROM THE REPLICA METHOD

An alternate way of justifying the DCA in the context of disordered systems is to use the replica (or other such) trick for disorder averaging.[19] This maps the disorder averaged problem into what looks like an interacting problem, and the DCA formalism developed by us earlier,[8,9] can simply be transcribed for this case, to arrive at the appropriate self-consistent cluster problem. For the effective cluster problem, the replica trick can be ''undone,'' and we recover the algorithm presented earlier in this paper. The same procedure also works for problems involving *both disorder and interactions*. We detail this below.

As is well known, for problems involving *quenched* disorder, as for example corresponding to the Hamiltonian:

$$H = H_0 + H_{\rm dis}, \tag{A1}$$

$$H_0 = \sum_{\mathbf{k},\sigma} \xi_{\mathbf{k}} C^{\dagger}_{\mathbf{k},\sigma} C_{\mathbf{k},\sigma}, \tag{A2}$$

$$H_{\rm dis} = \sum_{i\sigma} V_i n_{i,\sigma}, \tag{A3}$$

where $\xi_{\mathbf{k}} = \epsilon_{\mathbf{k}} - \mu$, and V_i is the random potential distributed according to a given probability distribution $P(V)$, complications arise because the disorder averaging has to be done on the *free energy*

$$F = -k_B T \ln Z$$

and the *Green functions*

$$G_{i,j}(\tau) = -\mathrm{Tr}[\mathbf{T}_\tau C_{i,\sigma}(\tau) C^{\dagger}_{j,\sigma} \exp(-\beta H)]/Z.$$

Here $Z = \mathrm{Tr}[\exp(-\beta H)]$ is the partition function, and $\mathbf{T}_\tau$ represents the imaginary-time ordering operator.

In the replica trick,[19] one writes

$$\ln Z = \lim_{m_r \rightarrow 0} \frac{Z^{m_r} - 1}{m_r} \quad \text{and} \quad 1/Z = \lim_{m_r \rightarrow 0} Z^{m_r - 1}$$

and *assumes* that the order of taking the limit $m_r \rightarrow 0$ and disorder averaging can be interchanged. Then for any positive integer m_r, the resulting disorder averaged quantities such as $\langle Z^{m_r} \rangle$, $\langle G_{\mathbf{k}}(\tau) \rangle$, etc., can be represented in terms of an *interacting* problem involving m_r replicas of the original electronic degrees of freedom, which we index with the subscript $\alpha = 1, \ldots, m_r$.

For example, using the standard Fermionic (Grassmann variable) functional integrals[20] to represent the traces above, we can write

$$\langle Z^{m_r} \rangle = \int D\, c^* D\, c \exp[-\beta \Psi], \tag{A4}$$

$$\langle G_{\mathbf{k}}(\tau) \rangle = -\int D\, c^* D\, c\, c_{\mathbf{k},\sigma,1}(\tau) c^*_{\mathbf{k},\sigma,1}(0) \exp[-\beta \Psi]. \tag{A5}$$

Here Ψ is an effective free-energy functional that arises from the disorder averaging, and can be written as

$$\beta \Psi = \sum_{\mathbf{k},\sigma,\alpha} \int_0^\beta d\tau\, c^*_{\mathbf{k},\sigma,\alpha}(\tau)(\partial_\tau + \xi_{\mathbf{k}}) c_{\mathbf{k},\sigma,\alpha}(\tau) + \sum_i^N W(\tilde{n}_i) \tag{A6}$$

where,

$$\tilde{n}_i \equiv \sum_{\alpha,\sigma} \int_0^\beta n_{i,\sigma,\alpha}(\tau) d\tau$$

and

$$\exp[-W(\tilde{n}_i)] = \langle \exp(-V_i \tilde{n}_i) \rangle = \int dV_i P(V_i) \exp(-V_i \tilde{n}_i).$$

In terms of the cumulants $\langle V^l \rangle_c$ of the disorder distribution $P(V)$, one can write

$$W(\tilde{n}_i) = \sum_{l=2}^{\infty} \frac{1}{l!} \langle V^l \rangle_c (\tilde{n}_i)^l.$$

So, clearly, W introduces (local in space but nonlocal in time) interactions between electrons belonging to arbitrary replicas.

If one re-expands $\exp[-W(\tilde{n}_i)]$ in powers of the cumulants $\langle V^l \rangle_c$ one can perform the Fermionic traces using the standard techniques of diagrammatic perturbation theory. Then, order-by-order in perturbation theory, the dependence on m_r is explicit and analytic, and the $\lim_{m_r \to 0}$ can be evaluated precisely. The resulting terms are in exact, one-to-one correspondence with the terms obtainable by writing out the diagrams from a direct perturbation expansion in powers of V_i and then disorder averaging as discussed in Sec. II. The $m_r \to 0$ limit eliminates the diagrams (in the interacting problem) containing internal loops with free sums over the replica indices (as required, since such diagrams never appear in the direct disorder averaged perturbation theory formalism of Sec. II).

For the ''replicated interacting problem'' obtained above, one can transcribe exactly the DCA formalism discussed in Refs. 8 and 9. If one assumes that the self-consistent host propagators do not break replica symmetry, then the effective cluster problem corresponds to a Fermionic functional integral involving an effective, self-consistent cluster free-energy functional given by

$$\beta \Psi_c = \sum_{\mathbf{K},\sigma,\alpha} \int_0^\beta d\tau \int_0^\beta d\tau' c^*_{\mathbf{K},\sigma,\alpha}(\tau) \times \mathcal{G}^{-1}(\mathbf{K}, \tau - \tau') c_{\mathbf{K},\sigma,\alpha}(\tau') + \sum_i^{N_c} W(\tilde{n}_i). \quad \text{(A7)}$$

But, as is easy to see using the same procedure as outlined earlier in this appendix, such an effective free-energy functional is exactly what one would obtain if one were to disorder average (using the replica trick) a cluster problem with N_c sites, which are dual to the cluster momenta $\mathbf{K}$, a bare (retarded) cluster propagator $\mathcal{G}^{-1}(\mathbf{K}, \tau - \tau')$, and a random potential V_i distributed according to $P(V_i)$ at every site i of the cluster. Hence we have an alternate justification for the disorder-DCA algorithm set down in Sec. III. The above route also enables one to quickly extend our discussions in Ref. 9 regarding the two-particle propagators, Ward identities, etc., to the disorder-DCA context. Most significantly, the DCA estimate of the lattice self-energy is minimized by the choice $\Sigma_\alpha(\mathbf{k}, \omega) = \overline{\Sigma}[\mathbf{M}(\mathbf{k}), \omega]$.

We note that the arguments presented in the main text and in this appendix are also easily extended to problems involving *interactions and disorder*. For example, for the case of the Hubbard model with diagonal disorder, one would add to the starting Hamiltonian the interaction term $U \Sigma_i^N n_{i,\uparrow} n_{i,\downarrow}$. Going through exactly the same procedures as outlined above, it is not hard to see that the only change is that the effective free-energy functionals for the lattice and the cluster pick up the additional terms $U \Sigma_\alpha \Sigma_{i^N} n_{i,\uparrow,\alpha} n_{i,\downarrow,\alpha}$ and $U \Sigma_\alpha \Sigma_{i^{N_c}} n_{i,\uparrow,\alpha} n_{i,\downarrow,\alpha}$. The resulting cluster problem now has both interactions and disorder on the cluster of N_c sites, which are dual to the cluster momenta $\mathbf{K}$: a bare (retarded) cluster propagator $\mathcal{G}^{-1}(\mathbf{K}, \tau - \tau')$, a random potential V_i distributed according to $P(V_i)$, and the Hubbard interaction U at every site i of the cluster. One can resort to any technique of one's choice to solve this problem for the disorder-averaged cluster Green's function $\overline{G}(\mathbf{K}, \omega)$ and cluster self-energies $\overline{\Sigma}(\mathbf{K}, \omega)$, and go through with the rest of the DCA iteration.

[1] P. Soven, Phys. Rev. **156**, 809 (1967); D. W. Taylor, *ibid.* **156**, 1017 (1967).

[2] For a review of developments through 1973, see the review article by R. J. Elliot, J. A. Krumhansk, and P. L. Leath, Rev. Mod. Phys. **46**, 465 (1974).

[3] For a detailed discussion of the CPA and earlier work on the inclusion of nonlocal corrections see A. Gonis, *Green Functions for Ordered and Disordered Systems*, in the series Studies in Mathematical Physics, edited by E. van Groesen and E. M. DeJager (North Holland, Amsterdam, 1992).

[4] B. L. Gyorffy, D. D. Johnson, F. J. Pinski, D. M. Nicholson, and D. M. Stocks, in *Proceedings of the NATO Advanced Study Institute on Alloy Phase Stability*, edited by G. M. Stocks and A. Gonis (Kluwer, Dordrecht, 1987), pp. 421–468; G. M. Stocks and H. Winters, in *Proceedings of the Nato Advanced Study Institute on Electronic Structure of Complex Systems*, edited by P. Phariseau and W. M. Temmerman (Plenum, New York, 1982), pp. 463–579.

[5] R. L. Mills and P. Ratnavararaksa, Phys. Rev. B **18**, 5291 (1978).

[6] T. Kaplan, P. L. Leath, L. J. Gray, and H. W. Diehl, Phys. Rev. B **21**, 4230 (1980).

[7] In particular, what are arguably the best of these extensions, namely, the TCA approach (Ref. 5) and its generalizations (Ref. 6) are designed to be causal, but are not systematic, in that the terms that are retained by them may be just as important as those dropped. Furthermore they are so hard to implement numerically that this has never been done for clusters larger than two sites.

[8] M. H. Hettler, A. N. Tahvildar-Zadeh, M. Jarrell, T. Pruschke, and H. R. Krishnamurthy, Phys. Rev. B **58**, 7475 (1998).

[9] M. H. Hettler, M. Mukherjee, M. Jarrell, and H. R. Krishnamurthy, Phys. Rev. B **61**, 12 739 (2000).

[10] Th. Maier, M. Jarrell, Th. Pruschke, and J. Keller, Eur. Phys. J. B **13**, 613 (2000).

[11] This same substitution was shown to serve as a diagrammatic definition of the dynamical mean-field theory. E. Müller-Hartmann, Z. Phys. B: Condens. Matter **74**, 507 (1989); **76**, 211 (1989).

[12] See D. F. Elliot and K. R. Rao, *Fast Transforms: Algorithms, Analyses, Applications* (Academic, New York, 1982).

[13] It is perhaps worth pointing out that the labor involved in solving Step 4 of the DCA cluster problem of size N_c is comparable to that of exactly solving a disordered open cluster or a disordered supercell of size N_c for the same distribution of disorder. The open cluster corresponds to fixing $\mathcal{G}(\mathbf{K})^{-1}=\omega-\epsilon_{\mathbf{K}}$. Whereas, in case of the supercell, wherein a distribution of disorder over a cluster of size N_c is periodically repeated, $\tilde{\mathbf{k}}$ will be a good quantum number, and for each separate value of $\tilde{\mathbf{k}}$, one has a disordered cluster problem with $\mathcal{G}(\mathbf{K})^{-1}=\omega-\epsilon_{\mathbf{K}+\tilde{\mathbf{k}}}$. However, the consequences of disorder averaging in the different treatments are radically different. This becomes especially clear if one contemplates what the approximations correspond to for $N_c=1$. While the DCA for $N_c=1$ reduces to the CPA, the (''disorder averaged'') supercell for $N_c=1$ would correspond to averaging the properties due to a periodic band, and the open cluster to averaging the properties of a sharp localized level, over the distribution of the chemical potential! Analogs of these differences would persist to finite N_c. The differences would show up even more glaringly in two particle properties. While the DCA provides a clean prescription leading to a finite conductivity, calculation of the conductivity for the disordered open cluster requires *ad hoc* smoothing procedures because of its inherently discrete spectrum, whereas the supercell would give divergent results for the conductivity because of its periodicity.

[14] J. E. Hirsch and R. M. Fye, Phys. Rev. Lett. **56**, 2521 (1986).

[15] D. J. Thouless, Phys. Rep. **13C**, 94 (1974).

[16] A. J. McKane and M. Stone, Ann. Phys. N.Y. **131**, 36 (1981).

[17] P. A. Lee and T. V. Ramakrishnan, Rev. Mod. Phys. **57**, 287 (1985).

[18] G. Bergmann, Phys. Rep. **107**, 1 (1984).

[19] F. Wegner, Z. Phys. B: Condens. Matter **35**, 207 (1979); L. Schafer and F. Wegner, *ibid.* **38**, 113 (1980); K. B. Efetov, A. I. Larkin, and D. E. Khemel'nitskii, Zh. Éksp. Teor. Fiz. **79**, 1120 (1980) [Sov. Phys. JETP **52**, 568 (1980)]; A. A. M. Pruisken and L. Schafer, Nucl. Phys. B **200**, 20 (1982).

[20] For example, see V. N. Popov, *Functional Integrals in Quantum Field Theory and Statistical Physics* (Reidel, Dordrecht, 1983).